

UDK 665.7.035.8

Structural and Electrical Properties of Ti Doped α -Fe₂O₃**M. V. Nikolic^{1*}, D. L. Sekulic², N. Nikolic¹, M. P. Slankamenac², O. S. Aleksic¹, H. Danninger³, E. Halwax³, V. B. Pavlovic⁴, P. M. Nikolic⁴**¹Institute for Multidisciplinary Research, University of Belgrade, Kneza Visislava 1, 11000 Beograd, Serbia²University of Novi Sad, Faculty of Technical Sciences, 21000 Novi Sad, Serbia³Institute of Chemical Technologies and Analytics, TU Wien, Getriedemarkt 9, Wien, Austria⁴Institute of Technical Sciences of SASA, Knez Mihailova 35, 11000 Beograd, Serbia**Abstract:**

In this work we have analyzed the effects of Ti doping on structural and electrical properties of α -Fe₂O₃. When the amount of added Ti (5 wt.%TiO₂) was within the solubility degree and XRD, SEM and EDS analysis revealed a homogenous hematite structure, with lattice parameters $a=5.03719(3)$ Å, $c=13.7484(1)$ Å slightly increased due to incorporation of Ti into the rhombohedral hematite lattice. Higher amounts of Ti (10 wt.%TiO₂) resulted in the formation of pseudobrookite, besides hematite, confirmed by SEM and EDS analysis. Studies of electric properties in the temperature range 25-225°C at different frequencies (100 – 1Mz) showed that Ti doping improved electrical conductivity. Impedance analysis was performed using an equivalent circuit, showing one relaxation process and suggesting dominant grain boundary contribution.

Keywords: X-ray diffraction, Scanning electron microscopy, Electric properties

1. Introduction

Semiconductor materials for economical production of hydrogen using solar energy have long been in focus, since the first report on hydrogen production on TiO₂ forty years ago [1]. However, though extensive experimental and theoretical research has been done on many potential materials, no single material has been found that meets all the required criteria: to be abundant, inexpensive, stable in aqueous solutions and yet have high solar-to-hydrogen conversion efficiency [2-5].

Hematite (α -Fe₂O₃) is an inexpensive, abundant, non-toxic material, stable in most alkaline electrolytes. It has a bandgap of 2.2 eV and can absorb approximately 40% of incident sunlight. However, it is a poor electronic material with low conductivity [6]. The photoelectrochemical performance of hematite can be improved by doping. More than 50 years ago Morin [7] studied the conduction mechanism of hematite doped with 0.05 to 1.0 at.% Ti. Substitutional doping of hematite has been investigated both theoretically and experimentally using dopants such as Si [7,8], Mo [9], Al [10-12], Zn [13], Sn [12, 14,16-18] and Ti [2,7,14-19] that significantly alter the electronic and physical properties of hematite. Some authors combine several dopants to balance the ion radius differences and enhance the

*) **Corresponding author:** mariav@rcub.bg.ac.rs

donor concentration, as is the case of Si and Ti codoped α -Fe₂O₃ analyzed by Zhang et al [20].

As hematite typically exhibits n-type indirect band gap semiconducting behaviour introduction of tetravalent ions into trivalent iron sites provides additional n-type doping [2]. Ti has been shown to be a potentially effective dopant for hematite thin films [2,7,14,15]. Thermoelectric properties of Ti doped hematite were investigated by Muta et al [19] and it was shown that addition of Ti increased electrical conductivity and decreased Seebeck coefficients. A combinatorial investigation of the effects of adding small amounts of Ti, Si and Al on the photoelectrochemical activity of α -Fe₂O₃ was investigated in [12] showing that low levels of Ti addition enhanced the photocurrents. Incorporation of Ti in thin films improved charge transport while decreasing recombination both in the bulk and on the surface of the film [14].

Titanium is a strong deoxidizer commonly used in steel making. It is a stabilizing and strengthening element [21]. Titanium forms a large number of stable oxides. The solubility of Ti in Fe₂O₃ is extensive with a homogeneity range from Fe₂O₃ (hematite) to FeTiO₃ (ilmenite), which at 1200°C extends slightly beyond ilmenite up to Fe_{0.97}Ti_{1.03}O₃. In the temperature range 800-1300°C the Fe₂O₃-TiO₂ binary system contains rhombohedral α -oxide (M₂O₃) involving mutual solubility of Fe₂O₃ and TiO₂, where up to TiO₂ incorporation changes with temperature from 16.3 mol% TiO₂ in Fe₂O₃ at 1300°C, 12.3 mol% at 1200°C, 8.4 mol% at 1100°C to 5 mol.% at 1000°C [22]. The second component is a rutile based TiO_{2-x} series, where the maximum solubility of Fe₂O₃ in rutile is ~0.8 mol% at 1200°C. The third component of the Fe₂O₃-TiO₂ system is ferric-pseudobrookite Fe₂TiO₅ [22]. At constant oxygen content of 62.5 at% this is another solid solution denoted M₃O₅ (M denotes Fe and Ti atoms, ideally pseudobrookite FeTi₂O₅) [21].

Velev et al [23] investigated the electronic and magnetic structure of transition-metal-doped α -hematite using the local density approximation with local correlations. When Ti substitutes Fe, three of the four valence electrons are taken by the surrounding oxygen atoms leaving one electron for Ti. According to the analysis made in [10,24] this extra electron converts a neighbouring Fe³⁺ ion to Fe²⁺ forming a donor level just below the Fermi energy. A density functional theory (DFT) study of 3d transition metals in hematite was also done by Huda et al [3] leading to the conclusion that incorporation of Ti provides electron carriers and reduces the electron effective mass, leading to potentially improved electrical conductivity of hematite and incorporation of this dopant could potentially lead to the greatest increase in electrical conductivity and therefore to the greatest enhancement of photoelectrochemical performance. Droubay et al [25] suggested from computational studies that for small degrees of substitution by Ti (in hematite) the decrease in band gap can be associated with the appearance of empty Ti d states just below, overlapping the conduction band minimum. They proposed that for higher levels of Fe substitution by Ti each electron is effectively localized on one Fe cation, reducing it from Fe³⁺ to Fe²⁺.

Gas sensing properties of iron-titanium oxide solid solutions were investigated in detail by Luthra et al [26]. The gas sensing behavior towards CO was found to be reasonably good within the solubility limit of the solid solution and sensitivity decreased due to the appearance of a secondary phase, agglomeration in the microstructure and formation of electron trap states associated with Fe²⁺ that can be related to segregation of Ti.

The purpose of this work was to analyze the effects Ti doping on structural and electrical properties of α -Fe₂O₃, by varying the amount of Ti above and below the solubility degree of Ti in α -Fe₂O₃.

2. Experimental

Hematite powder (purity 99.98%) was doped with titanium in fraction of 5 and 10 wt.% TiO₂ (rutile, purity 99.99%) and homogenized in a planetary ball mill for 15 minutes. Green samples 10 mm in diameter were sintered at 1200°C for two hours.

XRD analysis of sintered samples of Ti doped Fe₂O₃ was performed on a Panalytical X'Pert PRO system with CuK_α radiation and a graphite monochromator with a step scan of 0.02 s and holding time of 14 s in the 2θ range 5-135°. Unit cell parameters were first calculated by Le Bail full pattern profile fitting [27] and then further refined by the Rietveld method using the FullProf software suite [28]. Sample morphology was analyzed using scanning electron microscopy (JEOL JSM 6390 LV and TESCAN Electron Microscope VEGA TS 5130MM) and energy dispersive X-ray spectroscopy (Oxford Instruments INCA Penta FETX3).

Samples used for electrical conductivity measurements were prepared in the form of a sandwich electrode structure. Silver coatings were used as electrodes (ohmic contact). Impedance measurements were carried out in the frequency range 100 Hz to 1 MHz on a HP-4194A impedance/gain-phase analyzer using a HP-16047A test fixture in the temperature range 25-225°C (298-498K). A personal computer with in-house built software was used for acquisition of measured data.

3. Results and Discussion

3.1 Structural characterization

Analyses of XRD diffractograms of Ti doped Fe₂O₃ have shown that samples doped with 5 wt.% TiO₂ contain only the hematite phase (rhombohedral, $R\bar{3}c$), all Ti atoms have been incorporated in the hematite crystal lattice (fig 1a). Back scattering images and X-ray distribution maps of constituent elements of these samples show a homogenous distribution of Fe and Ti in the hematite structure (fig. 2). EDS analysis determined the average amount of Ti in Fe₂O₃ when doped with 5 wt% TiO₂ as 1.38 at% (2.15 wt%) that is within the solubility degree of Ti in Fe₂O₃.

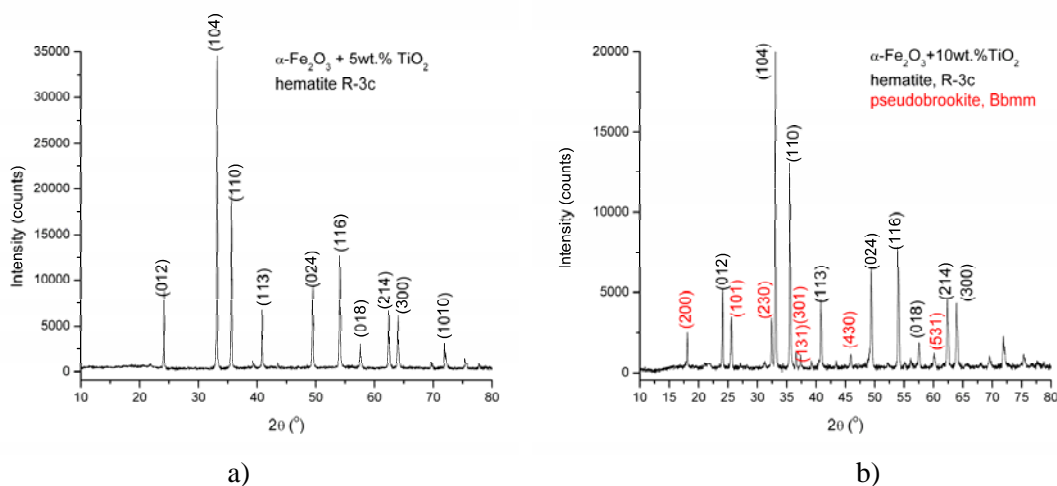


Fig. 1. X-ray diffractograms of Ti doped $\alpha\text{-Fe}_2\text{O}_3$

In the case of Fe₂O₃ samples doped with 10 wt% TiO₂ analysis of XRD diffractograms show the presence of two phases: hematite ($\alpha\text{-Fe}_2\text{O}_3$) and orthorhombic

pseudobrookite, FeTi_2O_5 (orthorhombic, $Bbmm$) (fig. 1b). EDS analysis determined the average amount of Ti in these samples as 5.67 at% (9.05 wt%). As XRD analysis has shown adding Ti above the solubility degree resulted in the formation of a secondary pseudobrookite phase that is in accordance with the results of Luthra et al [26]. Back scattering images, EDS analysis and X-ray distribution maps of constituent elements of these samples (fig. 3) showed that the distribution of elements was not homogenous, that is the consequence of the presence of two phases (hematite and pseudobrookite).

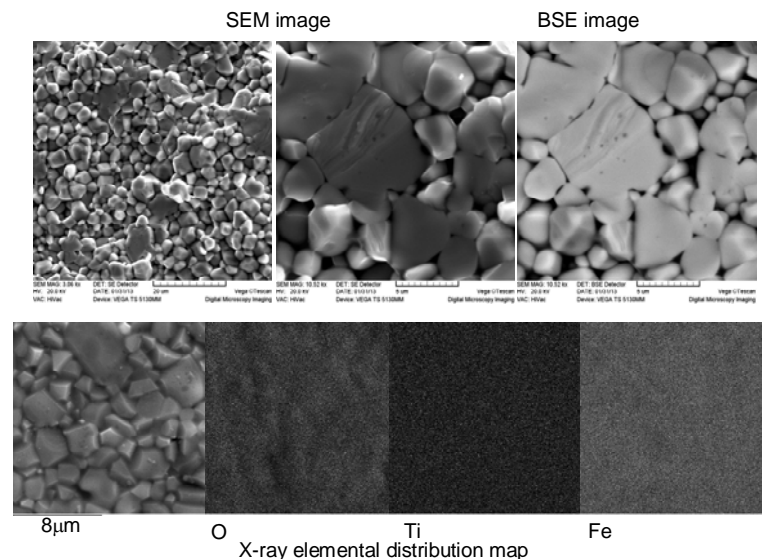


Fig. 2. SEM and BSE images and X-ray elemental distribution maps of O, Ti and Fe in $\alpha\text{-Fe}_2\text{O}_3$ samples doped with 5 wt.% TiO_2

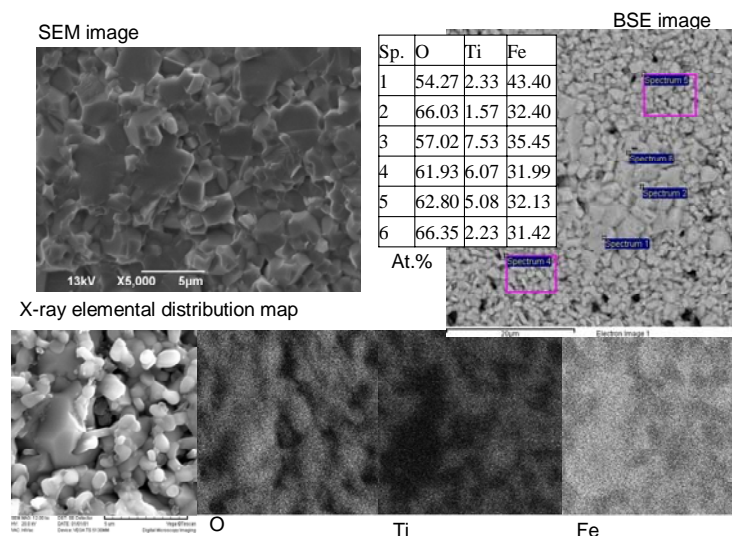


Fig. 3. SEM and BSE images, EDS analysis and X-ray elemental distribution maps of O, Ti and Fe in $\alpha\text{-Fe}_2\text{O}_3$ samples doped with 10 wt.% TiO_2

Lattice parameters determined for 5wt.% TiO_2 doped $\alpha\text{-Fe}_2\text{O}_3$ were $a=5.03719(3)$ Å, $c=13.7484(1)$ Å and $a=5.03873(5)$ Å and $c=13.75401(2)$ Å for $\alpha\text{-Fe}_2\text{O}_3$ and $a=9.798(1)$, $b=9.992(1)$ and $c=3.7138(2)$ for orthorhombic pseudobrookite, FeTi_2O_5 in 10wt.% TiO_2 doped $\alpha\text{-Fe}_2\text{O}_3$. If we compare the values obtained for lattice parameters for pure hematite $\alpha\text{-Fe}_2\text{O}_3$ samples obtained from the same starting powder and sintered in the same conditions as Ti doped samples, $a=5.03489(5)$ and $c=13.7389(2)$, and hematite with 5wt.% TiO_2 one can

note a slight increase due to Ti incorporation in the hematite lattice. This is in accordance with the findings of Muta et al [19]. In the case of hematite doped with 10 wt.% TiO_2 , the lattice parameters determined for the hematite phase are slightly higher. The in-plane and out-of-plane expansions are not very high and are still within literature values determined for pure hematite ($a=5.04 \text{ \AA}$ and $c=13.75 \text{ \AA}$ [30]). Even though one could expect that Ti substitution of Fe in the hematite lattice would cause lattice parameter contraction in both in-plane and out-of-plane directions, due to lower ionic radii of Ti^{4+} (0.61 \AA [31]) compared to Fe^{3+} (0.65 \AA [31]), this is not the case. Zhao et al [16] determined even more expressed changes in the case of Ti doped hematite films. They attributed these changes to the Ti doped hematite film becoming more ilmenite-like (ilmenite FeTiO_3 has a larger lattice $a=5.09 \text{ \AA}$, $c=14.08 \text{ \AA}$ [32]) and changes in elastic properties with increased Ti concentration.

3.2 Impedance analysis

Complex impedance plane plots at different temperatures for the analyzed samples of $\alpha\text{-Fe}_2\text{O}_3$ with 5 and 10 wt.% TiO_2 are shown in fig. 4. In fig. 4 for both sample types we can observe one semicircular arc, indicating one dominant relaxation phenomenon, suggesting a dominant role of the grain boundary contribution.

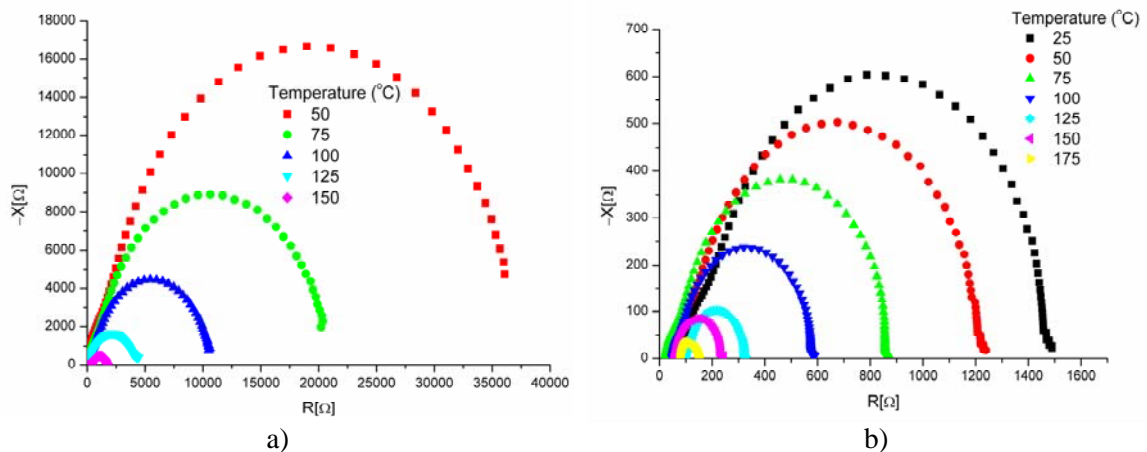


Fig. 4. Complex impedance plane plots at different temperatures for $\alpha\text{-Fe}_2\text{O}_3$ doped with 5 (a) and 10 (b) wt.% TiO_2

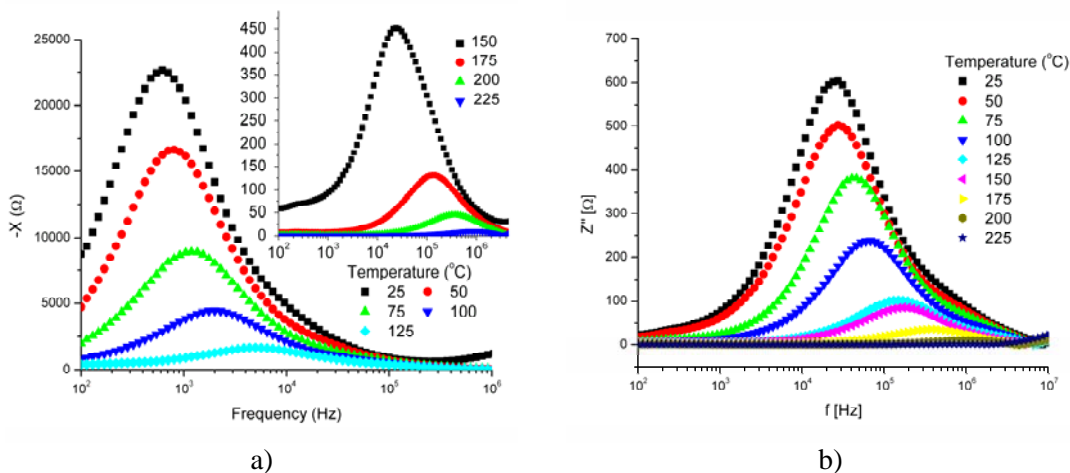


Fig. 5. Imaginary part of impedance (Z'') versus $\log(f)$ at different temperatures for $\alpha\text{-Fe}_2\text{O}_3$ doped with 5 (a) and 10 (b) wt.% TiO_2

One relaxation process can also be confirmed in the plot of imaginary part of the impedance (Z'') against the log of frequency at different temperatures (fig. 5). In both cases (samples with 5 and 10 wt.% TiO_2) one peak is observed and its frequency increases with increasing sample temperature. Impedance values obtained are much higher for hematite samples with less Ti, confirming that addition of Ti reduces resistivity, thus increasing conductivity. The decrease of the diameters of the semicircular arcs with temperature (in both cases) indicates the presence of a thermally activated conduction mechanism at grain boundaries. In the case of hopping, the carrier mobility is thermally activated and the carrier concentration is determined by the doping level [33].

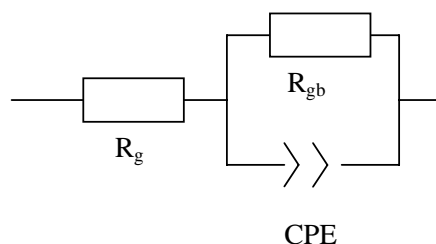


Fig. 6. Equivalent circuit

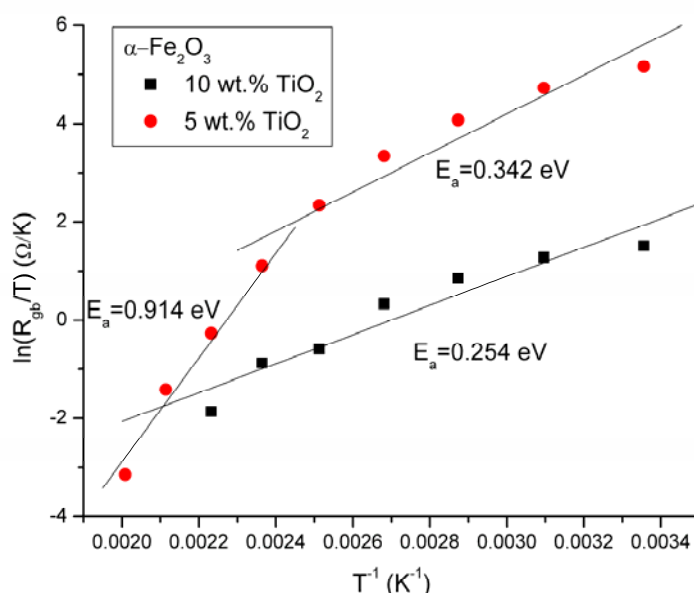


Fig. 7. Grain boundary resistance R_{gb} plotted against temperature using the adiabatic SPH model for $\alpha\text{-Fe}_2\text{O}_3$ doped with 5 and 10 wt.% TiO_2

Impedance data can be fitted and analyzed based on an idealized circuit model with discrete electrical components. In this case we used a simple equivalent circuit as shown in fig. 6, where R_g and R_{gb} represent the grain and grain boundary resistance. As the semicircles were depressed with a center below the real axis, then a constant phase element (CPE) was used to replace the capacitor C in the RC circuit [33-35]. CPE elements in the equivalent circuit model enable taking into account phenomena occurring in the interface regions, associated with inhomogeneity and diffusion processes. The impedance of a CPE can be described as [35]:

$$Z_{CPE} = A^{-1}(j\omega)^{-n} \quad (1)$$

where ω is the angular frequency, A and n ($0 \leq n \leq 1$) are fitted parameters. When the distributing factor $n=1$, then the CPE describes an ideal capacitor with $C = A$, while when $n=0$ the CPE describes an ideal resistor with $R=1/A$.

The real value of capacitance in the case when the capacitor is replaced with a CPE element in a RC circuit can be determined as [34]:

$$C_{CPE} = (A \cdot R^{-(n-1)})^{1/n} \quad (2)$$

where R , A and n are resistance and CPE parameter values determined from the applied model, respectively.

Analysis and simulation of impedance spectra was performed using EIS Spectrum Analyzer software [36]. The temperature dependence of the grain boundary resistance for hematite doped with 5 and 10 wt.% TiO_2 is given in fig. 7. It is plotted as $R_{gb}/T = A_o \exp(E_a/kT)$ using the adiabatic small polaron hopping (SPH) model [33], where A_o is the pre-exponential factor, k is the Boltzmann constant and E_a is the activation energy for conduction. In the case of samples (10 wt.% TiO_2) containing two phases – hematite and pseudobrookite, the determined activation energy for conduction at grain boundaries was 0.254 eV in the temperature interval 298-448 K (25-175°C), while in the case of samples containing only the hematite phase, the determined activation energy for conduction at grain boundaries was 0.342 eV in the temperature interval 298-398 K (25-125°C) and 0.914 eV in the higher temperature interval of 398-473 K (125-200°C).

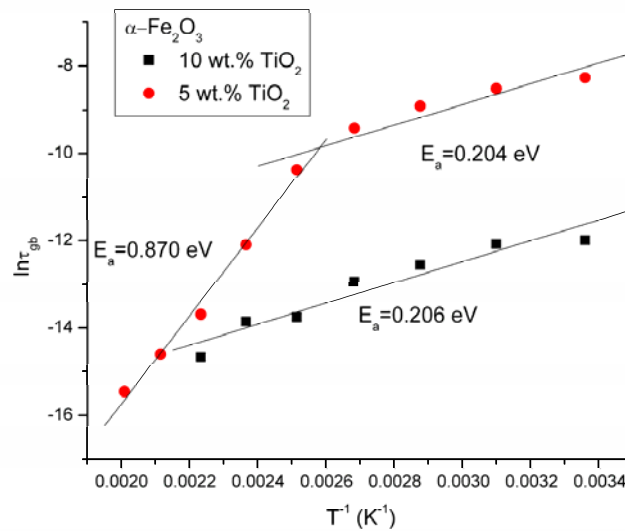


Fig. 8. Relaxation time τ_{gb} of the carriers at grain boundaries plotted against temperature using the inverse temperature dependence for $\alpha\text{-Fe}_2\text{O}_3$ doped with 5 and 10 wt.% TiO_2

The grain boundary relaxation time was calculated as $\tau_{gb} = 1/2\pi f_{gb}$ and its temperature dependence was plotted as $\tau_{gb} = \tau_0 \exp(E_{gb}/kT)$ in fig. 8, where τ_0 is the pre-exponential factor, k is the Boltzmann constant, E_{gb} is the activation energy for the relaxation process at grain boundaries and T is the temperature. In both sample types the grain boundary relaxation time decreases with temperature. In the case of samples with a higher Ti content (10 wt.% TiO_2) the activation energy in the temperature interval 298-448 K was determined as 0.206 eV. In the case of samples with a lower Ti content, the activation energy for grain boundary relaxation process was 0.204 eV in the temperature interval 298-398K and 0.870 eV in the temperature interval 398-473 K. This is similar to the results obtained for activation energy for conduction at grain boundaries. The small differences in values of activation energies for the conduction and relaxation may be due to the fact that the relaxation process involves only the hopping energy of carriers between the localized states, while the conduction mechanism involves hopping energy and also disorder and binding energy of

polarons [33]. The same type of charge carrier is responsible for both relaxation and conduction processes.

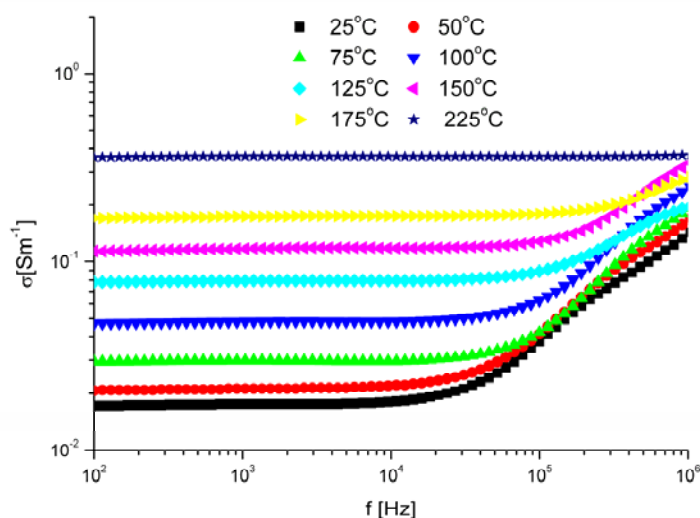


Fig. 9. Frequency dependence of ac conductivity for α -Fe₂O₃ doped with 10 wt.% TiO₂

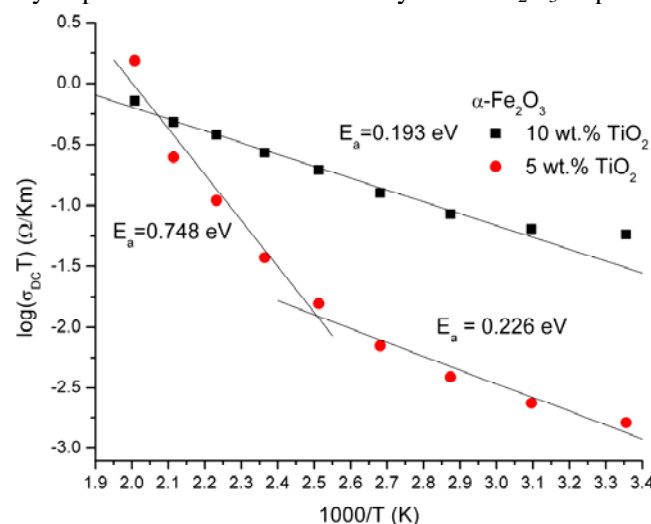


Fig. 10. DC conductivity as a function of temperature for α -Fe₂O₃ doped with 5 and 10 wt.% TiO₂

The frequency dependence of *ac* conductivity at various temperatures is shown in fig.9 for a α -Fe₂O₃+10wt.%TiO₂ sample. At each temperature at low frequencies there is a frequency independent region followed by a region where conductivity increases with frequency. This shows that the *ac* conductivity follows Jonscher's power law [37]: $\sigma_{AC} = \sigma_{DC} + A\omega^s$ that is typical for hopping conduction and where σ_{DC} is the *dc* conductivity, *A* and *s* are temperature dependent constants. Samples of α -Fe₂O₃+5wt.%TiO₂ behave in a similar way and changes of *ac* conductivity with frequency obey Jonscher's power law. If hopping of charge carriers is responsible for electrical conductivity then the relation between $(\sigma_{DC}T)$ and $(1/T)$ is linear and this is consistent with the Mott model for phonon-assisted hopping of small polarons in the adiabatic limit [38]. Carrier mobility is temperature dependent and the increase in *dc* conductivity with temperature is due to the increase in thermally activated drift mobility of charge carriers. Variation of the *dc* electrical conductivity with temperature for both sample types is shown in fig. 10. In the case of α -

$\text{Fe}_2\text{O}_3+10\text{wt.}\% \text{TiO}_2$ samples the activation energy was determined as $E_a=0.193$ eV in the temperature interval 298-498 K, while in the case of $\alpha\text{-Fe}_2\text{O}_3+5\text{wt.}\% \text{TiO}_2$ samples it was 0.226 eV in the temperature interval 298-398 K and 0.748 eV in the temperature interval 398-498 K.

If we analyze the activation energy values obtained for $\alpha\text{-Fe}_2\text{O}_3+10\text{wt.}\% \text{TiO}_2$ samples, namely activation energy for conduction at grain boundaries, activation energy for relaxation and also activation energy for conduction, one can see that these values were between 0.193 and 0.254 and included the complete analyzed temperature interval. The values are consistent with conduction induced by hopping of carriers, in this case electron hopping between Fe^{2+} and Fe^{3+} . Investigations of Ti doping of $\alpha\text{-Fe}_2\text{O}_3$ have shown that higher levels of Fe substitution by Ti each electron is effectively localized on one Fe cation, reducing it from Fe^{3+} to Fe^{2+} [25], improving conduction by increasing the number of Fe^{2+} and Fe^{3+} pairs responsible for conduction. Thus, in our samples with Ti substitution above the solubility degree in $\alpha\text{-Fe}_2\text{O}_3$, resulting in the formation of pseudobrookite, besides the hematite phase, lead to enhanced conductivity.

In the case of samples with lower Ti substitution, we obtained homogenous single phase samples, where Ti was incorporated into the hematite structure. In the analyzed temperature interval (298-498 K), at 398 K there was a change in the conduction-relaxation mechanism, as two values of activation energy were determined for conduction at grain boundaries, relaxation and also conduction. Oxygen vacancies and space charge may be responsible for these changes [39].

4. Conclusion

Structural analysis (XRD, SEM and EDS) revealed that due to the high solubility degree of Ti in $\alpha\text{-Fe}_2\text{O}_3$ addition of small amounts of Ti resulted in a homogenous hematite structure, with slightly increased lattice parameters $a=5.03719(3)$ Å, $c=13.7484(1)$ Å. Addition of Ti above the solubility degree resulted in the formation of pseudobrookite ($a=9.798(1)$, $b=9.992(1)$ and $c=3.7138(2)$), besides hematite ($a=5.03873(5)$ Å and $c=13.75401(2)$ Å), confirmed by SEM and EDS analysis. Complex impedance plane plots at different temperatures for the analyzed samples of $\alpha\text{-Fe}_2\text{O}_3$ with 5 and 10 wt.% TiO_2 showed a single relaxation process and dominant grain boundary contribution. Impedance data was analyzed using an equivalent circuit, enabling determination of activation energy for conduction at grain boundaries and activation energy for relaxation at grain boundaries. Values determined for activation energy for conduction showed that conduction was due to electron hopping between Fe^{2+} and Fe^{3+} , enhanced by Ti substitution.

Acknowledgement

This research was performed within projects III45014 and III43008 financed by the Ministry for Science, Education and Technological Development of the Republic of Serbia.

5. References

1. A. Fujishima, K. Honada, Nature 238 (1972) 37.
2. P. Zhang, A. Kleiman-Shwarscstein, Y.-S. Hu, J. Lefton, S. Sharma, A. J. Forman, E. McFarland, Oriented Ti doped hematite thin film as active photoanodes synthesized by facile APCVD, Energy Environ. Sci. 4 (2011) 1020-1028

3. M. N. Huda, A. Walsh, Y. Yan, S.-H. Wei, M. M. Al-Jassim, Electronic, structural and magnetic effects of 3d transition metals in hematite, *J. Appl. Phys.* 107 (2010) 123712.
4. M. Graetzel, Photoelectrochemical cells, *Nature* 414 (2001) 338-344.
5. X. C. Wang, K. Maeda, A. Thomas, K. Takanabe, G. Xin, J. M. Carlsson, K. Domen, M. Antonietti, A metal-free polymeric photocatalyst for hydrogen production from water under visible light, *Nature Materials* 8 (2009) 76-88.
6. F. J. Morin, Electrical properties of $\alpha\text{Fe}_2\text{O}_3$ and $\alpha\text{Fe}_2\text{O}_3$ containing titanium, *Phys. Rev.* 83 (1951) 1005-1010.
7. J. A. Glasscock, P. R. F. Barnes, I. C. Plumb, N. Savvides, Enhancement of photoelectrochemical hydrogen production from hematite thin films by the introduction of Ti and Si, *J. Phys. Chem. C* 111 (2007) 16477-16488.
8. I. Cesar, A. Kay, J. A. Gonzales Martinez, M. Graetzel, Translucent thin film Fe_2O_3 photoanodes for efficient water splitting by sunlight: nanostructure-directing effect of Si-doping, *J. Am. Chem. Soc.* 128 (2006) 4582-4583.
9. A. Kleiman-Shwarsstein, Y.-S. Hu, A. J. Forman, G. D. Stucky, E. W. McFarland, Electrodeposition of $\alpha\text{-Fe}_2\text{O}_3$ doped with Mo or Cr as photoanodes for photocatalytic water splitting, *J. Phys. Chem. C* 112 (2008) 15900-15907.
10. A. Kleiman-Shwarsstein, M. N. Huda, A. Walsh, Y. Yan, G. D. Stucky, Y.-S. Hu, M. M. Al-Jassim, E. W. McFarland, Electrodeposited aluminium-doped $\alpha\text{-Fe}_2\text{O}_3$ photoelectrodes: experiment and theory, *Chem. Mater.* 22 (2010) 510-517.
11. S. S. Shinde, C. H. Bhosale, K. Y. Rajpure, Studies on morphological and electrical properties of Al incorporated combusted iron oxide, *J. Alloys Compd.* 509 (2011) 3943-3951.
12. J. He, B. A. Parkinson, Combinatorial investigation of the effects of the incorporation of Ti, Si and Al on the performance of $\alpha\text{-Fe}_2\text{O}_3$ photoanodes, *ACS Comb. Sci.* 13 (2011) 399-404.
13. W. B. Ingler, J. P. Baltrus, S. U. M. Khan, Photoresponse of p-type zinc-doped iron (III) oxide thin films, *J. Am. Chem. Soc.* 126 (2004) 10238-10239.
14. N. T. Hahn, C. B. Mullins, Photoelectrochemical performance of nanostructured Ti- and Sn-doped $\alpha\text{-Fe}_2\text{O}_3$ photoanodes, *Chem. Mater.* 22 (2010) 6474-6482.
15. S. Kumari, A. P. Singh, Sonal, D. Deva, R. Shrivastav, S. Dass, V. R. Satsangi, Spray pyrolytically deposited nanoporous Ti^{4+} doped hematite thin films for efficient photoelectrochemical splitting of water, *Int. J. Hydrogen Energ.* 35 (2010) 3985-3990.
16. B. Zhao, T. C. Kaspar, T. C. Droubay, J. McCloy, M. E. Bowden, V. Shutthanandan, S. M. Heald, A. A. Chambers, Electrical transport properties of Ti-doped $\text{Fe}_2\text{O}_3(0001)$ epitaxial films, *Phys. Rev. B* 84 (2011) 245325.
17. F. J. Berry, C. Greaves, O. Helgasson, J. McManus, H. M. Palmer, R. T. Williams, Structural and magnetic Properties of Sn-, Ti- and Mg-substituted $\alpha\text{-Fe}_2\text{O}_3$: A study by neutron diffraction and Mossbauer spectroscopy, *J. Solid State Chem.* 151 (2000) 157-162
18. F. J. Berry, A. Bohorquez, E. A. Moore, Rationalization of defect structure of tin- and titanium-doped $\alpha\text{-Fe}_2\text{O}_3$ using interatomic potential calculations, *Solid State Communications* 109 (1999) 207-211.
19. H. Muta, K. Kurosaki, M. Uno, S. Yamanaka, Thermoelectric properties of Ti- and Sn-doped $\alpha\text{-Fe}_2\text{O}_3$, *J. Alloys Compd.* 335 (2002) 200-202.
20. M. L. Zhang, W. J. Luo, Z. S. Li, T. Yu, Z. G. Zou, Improved photoelectrochemical responses of Si and Ti codoped $\alpha\text{-Fe}_2\text{O}_3$ photoanode films, *Applied Physics Letters* 97 (2010) 042105.

21. V. Raghavan Phase diagrams of ternary iron alloys, Monograph Series on Alloy Phase Diagrams, Part 5, The Indian Institute of Metals, 1989, 300-323.
22. M. I. Pownceby, K. K. Constanti-Carey, M. J. Fisher-White, Subsolidus phase relationships in the system $\text{Fe}_2\text{O}_3\text{-Al}_2\text{O}_3\text{-TiO}_2$ between 1000 and 1300°C, J. Am. Ceram. Soc. 86 (2003) 975-980.
23. J. Velev, A. Bandyopadhyay, W. H. Butler, S. Sarker, Electronic and magnetic structure of transition-metal-doped α -hematite, Phys. Rev. B 71 (2005) 205208.
24. A. Bandyopadhyay, J. Velev, W. H. Butler, S. K. Sarker, O. Bengone, Effect of electron correlations on the electronic and magnetic structure of Ti-doped α -hematite, Phys. Rev. B 69 (2004) 174429.
25. T. Droubay, K. M. Rosso, S. M. Heald, D. E. McCready, C. M. Wang, S. A. Chambers, Structure, magnetism and conductivity in epitaxial Ti-doped $\alpha\text{-Fe}_2\text{O}_3$ hematite: Experiment and density functional theory calculations, Phys. Rev. B 75 (2007) 104412
26. V. Luthra, K. F. E. Pratt, R. G. Palgrave, D. E. Williams, R. P. Tandon, I. P. Parkin, Gas-sensing properties of $\text{Fe}_{2-x}\text{Ti}_x\text{O}_{3+y}$ ($x=0\text{-}1.4$), Polyhedron, 29 (2010) 1225-1230
27. A. Le Bail, H. Duroy, J. L. Fourquet, Ab-initio structure determination of LiSbWO_6 by X-ray powder diffraction, Mater. Res. Bull. 23 (1988) 447-452.
28. J. Rodriguez-Carvajal, Recent advances in magnetic structure determination by neutron powder diffraction, Physica B 192 (1993) 55-69.
29. S. Lanfredi, R. L. Grosso, A. C. Antunes, M. A. L. Nobre, High temperature behavior of alpha- Fe_2O_3 ceramic thermistor with negative temperature coefficient, Ceramica 54 (2008) 443-450
30. E. N. Maslen, V. A. Streltsov, N. R. Streltsova, N. Ishizawa, Acta Crystallogr. Sect. B-Struct. Commun. 50 (1994) 435
31. R. D. Shannon, Acta. Cryst. A 32 (1976) 751
32. B. A. Wechsler, C. T. Prewitt, Am. Mineral. 69 (1984) 176
33. M. Idrees, M. Nadeem, M. M. Hassan, Investigation of conduction and relaxation phenomena in $\text{LaFe}_{0.9}\text{Ni}_{0.1}\text{O}_3$ by impedance spectroscopy, J. Phys. D: Appl. Phys 43 (2010) 155401
34. M. V. Nikolic, M. P. Slankamenac, N. Nikolic, D. L. Sekulic, O. S. Aleksic, M. Mitric, T. Ivetic, V. B. Pavlovic, P. M. Nikolic, Study of dielectric behavior and electrical properties of hematite $\alpha\text{-Fe}_2\text{O}_3$ doped with Zn, Sci. Sintering, 44 (2012) 307-321
35. R. Martinez, A. Kumar, R. Palai, J. F. Scott, R. S. kattiyar, J. Phys. D:Appl. Phys. 44 (2011) 105302.
36. A. S. Bondarenko, G. Ragoisha, EIS Spectrum Analyzer, <http://www.abc.chemistry.bsu.by>
37. A. K. Jonscher, Nature 267 (1977) 673.
38. N. F. Mott, Conduction in glasses containing transition metal ions, J. Non-Cryst. Solids 1 (1968) 1-17.
39. S. K. Patri, R. N. P. Choudhary, B. K. Samantaray, Studies of structural, dielectric and impedance properties of $\text{Bi}_9\text{Fe}_5\text{Ti}_3\text{O}_{27}$ ceramics, J. Electroceram. 20 (2008) 119-126.

Садржај: У овом раду анализиран је утицај допирања титаном на структурна и електрична својства хематита. Када је количина додатог Ti (5 wt.% TiO_2) била у опсегу растворљивости, рентгенска, СЕМ и ЕДС анализе су показале хомогену хематитну структуру, са незнатно увећаним параметрима решетке $a=5.03719(3)\text{ \AA}$, $c=13.7484(1)\text{ \AA}$ услед присуства Ti у ромбоударској хематитној решетки. Веће

количине Ti (10 wt.%TiO₂) довеле су до формирања псеудобрукита, осим хематита, што је и потврђено СЕМ и ЕДС анализом. Проучавање електричних својстава у температурном опсегу 25-225°C на различитим фреквенцијама (100 – 1 Мз) показало је да допирање титаном побољшава електричну проводност. Анализа импедансе је извршена коришћењем еквивалентног кола, показујући један релаксациони процес који претпоставља доминацију утицаја граница зрна.

Кључне речи: Рентгенска дифракција, СЕМ микроскопија, електрична својства.
